

We are IntechOpen, the world's leading publisher of Open Access books Built by scientists, for scientists

6,900

Open access books available

186,000

International authors and editors

200M

Downloads

Our authors are among the

154

Countries delivered to

TOP 1%

most cited scientists

12.2%

Contributors from top 500 universities



WEB OF SCIENCE™

Selection of our books indexed in the Book Citation Index
in Web of Science™ Core Collection (BKCI)

Interested in publishing with us?
Contact book.department@intechopen.com

Numbers displayed above are based on latest data collected.
For more information visit www.intechopen.com



Micro-Rheological Study on Fully Exfoliated Organoclay Modified Thermotropic Liquid Crystalline Polymer and Its Viscosity Reduction Effect on High Molecular Mass Polyethylene

Youhong Tang and Ping Gao

Additional information is available at the end of the chapter

<http://dx.doi.org/10.5772/45996>

1. Introduction

Molten thermotropic liquid crystalline polymers have physical properties that are dependent on both small molecule liquid crystals and flexible chain polymers. Liquid crystalline polymers (LCPs) are typical examples of self-ordered polymeric systems, due largely to their intrinsic molecular anisotropy. The properties of LCPs are strongly influenced by flow-induced changes in the degree of molecular orientation during processing [1].

Blends containing small amounts of a thermotropic liquid crystalline polymer (TLCP) in a matrix of thermoplastic have attracted technical interest in recent years for two main reasons. Firstly, by the use of TLCP to enhance the mechanical properties of the matrix polymer through in situ formation of fibrous TLCP dispersion during processing, it may be possible to develop 'self-reinforced' composites that exploit the outstanding tensile properties of fibres made from LCPs. Secondly, it is known that TLCP can act as a flow modifier, resulting in a substantial reduction in pressure drop during melt extrusion. Previous studies by Chan et al.[2] have shown that a small amount of TLCP (1.0 wt %) added to high molecular weight polyethylene (HMMPE, Chevron Phillips Marlex® HXM TR570) caused drastic bulk viscosity reduction (> 95.0%) to occur at 190 °C, when TLCP was in its nematic phase. A significant improvement in extrudate surface smoothness has also been observed, coupled with an increase in the processing window from 34 1/s to up to 1000 1/s. Whitehouse et al. [3] blended 0.2%, 0.5% and 2.0% TLCP with high density polyethylene (HDPE, Chevron Phillips Marlex® HMN 6060), and the blends were then rheologically

characterized at 185 °C when the TLCP was in the nematic regime; substantial viscosity reductions of between 85% and 90% compared with pure HDPE were observed.

It is worth noting that even in early studies of polymer blends containing TLCP, researchers had already attempted to introduce inorganic reinforcements into such blend systems [4]. The addition of inorganic fillers not only enhanced the mechanical properties of the blends but also reduced the anisotropy of the resulting materials [5]. Rheological characterization revealed that TLCP could reduce the melt viscosity of glass-filled thermoplastics [6]. Much work has been published on TLCP systems containing different inorganic solid reinforcements, such as glass fibres [7], carbon black [8], whiskers [9] and silica [10]. Most of the studies have used high inorganic solid reinforcement content and have focused on the balance between the mechanical properties and processability of such blends.

Layered silicates have long been used as fillers in polymeric systems to improve mechanical, thermal and other properties in the resulting polymer composites. In layered silicate itself, the local interaction between layers causing the presence of domains similar to those found in studies of liquid crystalline and ordered block copolymer systems have been analyzed by many researchers [11-14].

It seems that intercalation or exfoliation of layered silicates in polymers should induce nanocomposites to exhibit similar rheological behaviour to that found in the nematic state structures in LCPs. Nanocomposites based on thermotropic liquid crystalline polymer and organically modified layered silicate have been studied by several groups with different foci. Zhang et al. [15] synthesized a series of liquid-crystalline copolyester/organically modified montmorillonite nanocomposites by intercalation polycondensation with different surfactant modified clay in LCP. X-ray diffraction and transmission electron microscope studies indicated that, after ion exchange with suitable surfactants, clay formed delaminated morphology and was well dispersed in LCP. Chang et al. [16] reported nanocomposites of TLCP with an alkoxy side-group and an organoclay (Cloisite 25 A) prepared by the melting intercalation method above the melt transition temperature of TLCP, with liquid crystallinity of the hybrids being lost when the organoclay content exceeded 6.0 %. Vaia et al. [17] directly annealed a powder mixture of TLCP and clay within the nematic region of TLCP under high hydraulic pressure. Reversible intercalation formed, with a loss of liquid crystallinity which was attributed to the confinement of LCP chains on the clay pseudo-2D geometry. An extensive study of a series of nanocomposites with a segmented main-chain liquid crystalline polymer having a pendent pyridyl group (PyHQ12) or a pendent phenylsulfonyl group (PSHQ12) and commercial Cloisite 20 A or 30B clays by examining rheological and other properties was reported by Huang and Han [18, 19] to demonstrate whether functionality of TLCP was essential to obtain highly dispersed clay in nanocomposites with TLCP as matrix. Only intercalated morphology formed when the nanocomposites were based on a TLCP without functionality. The formation of hydrogen bonds caused a very high degree of dispersion but a considerable loss in the degree of liquid crystallinity in a PyHQ12/30B nanocomposite. From the above studies, it can be seen that functionality in TLCP is necessary to obtain highly dispersed nanocomposites, but at the same time, there is the possibility of loss some degree of liquid crystallinity in the TLCP.

In this study, the organoclay-modified TLCP (TC3 white) is prepared by a method combining ultra-sonication, centrifugation, solution casting and heating-shearing separation. TC3 white has a very high degree of dispersion of organoclay but without any loss in the degree of liquid crystallinity of TLCP. The effects of the fully exfoliated organoclay on the thermal and rheological properties of TLCP are investigated in detail. Based on this material, we characterize the rheological behaviour of purified TLCP and TC3 white with 1 wt% in HMMPE matrix by a capillary rheometer at 190 °C and 230 °C, where the TLCP has its nematic and nematic-isotropic biphasic structures. Schematic drawings of the conformation of organoclay, TLCP molecules and polyethylene molecules before and after yielding are shown. A binary flow pattern model with simulated results is presented and the predicted results show good consistency with experimental data.

2. Experimental

2.1. Materials and samples preparation

2.1.1. Materials

The HMMPE, Chevron Phillips Marlex® HXM TR571, with a melt flow index (MFI) of 2.5g/10 min (ASTM D1238, 190 °C/21.6 kg) was kindly supplied by Phillips Petroleum International Inc., USA. The TLCP, a copolymer containing 30% p-hydroxybenzoic acid, 35% hydroquinone and 35% sebacic acid (HBA/HQ/SA), used here was synthesized and kindly supplied by B. P. Chemicals Ltd, UK. The as-received TLCP is a light brown powder that has been characterized previously [20]. The Organoclay, Closite 20A modified by dimethyl dihydrogenated tallow ammonium ions, was kindly supplied by Southern Clay Products.

2.1.2. Purification of as-received TLCP

The as-received dried TLCP powder was dissolved into chloroform and followed by mechanically stirred at room temperature overnight. The deionized water was added to the mixture and was mechanically stirred for several minutes. Water extraction was repeated several times to remove any water soluble content, e.g. pure sebacic acid; the subsequent solution was subjected to centrifugal separation (KUBOTA 2010, Japan) at a speed of 3,800 rpm for 1800 seconds. Three layers of solution were obtained. The bottom layer was a brownish precipitate which was believed to be a mixture of HBA, HBA rich TLCP, catalyst or other heavier components in the TLCP powder. The top layer was a white cloudy layer, which was believed to be a SA rich TLCP component. The middle colorless portion was extracted. To obtain more thorough purification, the whole centrifugal separation and extraction processes were repeated several times. The TLCP powder was precipitated out by dropping the extracted solution into methanol. The TLCP fine powder was filtered out and dried at 120 °C for 3 days to remove any residual solvent contents.

2.1.3. Organoclay-modified as-received TLCP (TC3 white) preparation

Initially, TLCP was dried in a vacuum oven at 120 °C for 2 days and organoclay in an oven at 100 °C overnight. The materials were dissolved and dispersed in chloroform respectively with a TLCP/organoclay weight ratio 97:3. The solutions were then stirred for about 4 hours at room temperature. After that, TLCP and organoclay were mixed together and the mixture was sonicated by ultrasonic pin vibration (Branson digital sonifier 450, USA) with 45% power for about 2 hours at room temperature. Subsequently, the mixture was centrifuged with a speed of 3,800 rpm for 45 minutes to separate the bottom layer precipitate which was believed to be redundant organoclay and unsolvable TLCP, and the top layer, if any, which was believed to be impurities in TLCP, from the middle portion; then the solvent was volatilized at room temperature. A nanocomposite was obtained, which was dried in an oven at 60 °C for 12 hours and in a vacuum oven at 120 °C for 2 days. The nanocomposite showed severe shear-induced phase separation phenomenon at 190 °C or higher temperatures and can be effectively separated by a capillary rheometer at 190 °C at a low speed (5.0 1/s) [21]. The extruded material was named TC3 white because of its white color, which will be used here for study.

2.1.4. Polyethylene blends preparation

For HMMPE blends, the dried 1.0 wt% TC3 white (or purified TLCP) in powder form and HMMPE in pellet form were mechanically pre-mixed at room temperature until macroscopically homogeneous. The mixture was then extruded using a Dr. Collin twin screw extruder (Dr. Collin GMBH, Germany) at 190 °C with two-time extrusion at different speeds (75 rad/s and 300 rad/s respectively). The extrudate was palletized and kept dry inside an oven overnight to remove moisture generated during the process.

2.2. Characterizations

2.2.1. Wide angle X-ray diffraction

Wide angle X-ray diffraction (WAXD) was conducted at room temperature on a Philips powder X-ray diffraction system (Model PW 1830, The Netherlands). TLCP and TC3 white were first dried in a vacuum oven for 2 days, then hot pressed at 170 °C to form films with thickness of 300 μm ; the organoclay was characterized in powder form. WAXD was conducted with Cu $k\alpha$ radiation of wavelength 1.5406 Å .

2.2.2. Fourier transform infraRed & nuclear magnetic resonance spectra

A Fourier transform infrared (FTIR) spectrometer (Bio-Rad FTS 6000, USA) was used at room temperature with a liquid cell container for solutions. Spectral resolution was maintained at 2 cm^{-1} . Dry nitrogen gas was used to purge the sample compartment to reduce the interference of water and carbon dioxide in the spectrum. The solutions were the TLCP chloroform and the TLCP/organoclay chloroform solutions before evaporation

procedure. The ^{13}C nuclear magnetic resonance (NMR) spectra were measured at room temperature on a Bruker ARX 300 NMR spectrometer using chloroform-d as the solvent, and the chemical shifts were reported on the δ scale using tetramethylsilane (TMS) as the internal reference.

2.2.3. Polarized optical microscopy

The mesophase structures of the liquid-crystalline phase of TLCP and its nanocomposite were investigated by polarized optical microscopy (POM) using an Olympus microscope BX 50 with a Cambridge shear system CSS450 connecting a hot stage. The most outstanding feature of this setup is that it allows investigation of texture changes at different temperatures and under varying shear rates. Mesophase structure images were obtained at 185 °C after preshearing samples with a low shear rate i.e. 0.5 1/s for more than 3600 seconds to remove any shear history and anchored defects, and to give a common shear history or structure to samples before isothermal treatment in a quiescent condition for sufficient time.

2.2.4. Thermogravimetric analysis & differential scanning calorimetry

Thermal stability analysis was carried out by using a Hi-Res TGA 2950 thermogravimetric analysis (TGA) apparatus (TA instruments, USA). The test was carried out in air with a heating rate of 20.0 °C/min from 50.0 °C to 600.0 °C, and then isothermally treated for 30 minutes at 600.0 °C. The phase transition temperature of the nanocomposite based on TLCP was determined via differential scanning calorimetry (DSC) (PYRIS diamond DSC, Perkin-Elmer Instruments, USA), using indium as the calibration standard, with heating or cooling rate of 10.0 °C/min under nitrogen atmosphere.

2.2.5. Advanced rheometric expansion system and capillary rheometer

Controlled strain rheological measurements were carried out using an advanced rheometric expansion system (ARES) (TA instruments, USA) with a 200 g-cm transducer within the resolution limit of 0.02 g-cm. 50 mm cone and plate fixtures with nominal cone angle 0.04 rad and nominal gap 0.0508 mm, as well as 50 mm parallel plate fixtures were used for TLCP and its nanocomposite reported here. All measurements were performed at 185 °C in N_2 atmosphere, where TLCP had been shown to exhibit stable rheological properties under the nematic phase. Care was taken to ensure a controlled thermomechanical history as follows: the rheometer was heated to the testing temperature and allowed to reach equilibrium. Fresh samples, dried in a vacuum oven for 2 days at 120 °C, were loaded in the preheated rheometer, heated up to 185 °C then held for 10 minutes. Decreased gap to the testing gap and kept isotherm for 30 minutes to reach thermal and deformation equilibrium before measurements were started. The experiments were repeated no less than three times to check reproducibility. In each case, a fresh sample was used. For all tests reported here on HMMPE blends, 25 mm parallel plate fixtures were used. All measurements were performed at 190 °C with a 2000 g-cm transducer within the

resolution limit of 0.2 g-cm and a 200 g-cm transducer within the resolution limit of 0.02 g-cm. Before testing, equipment was preheated and equilibrated at the test temperature for at least 30 minutes [22].

The rheological behaviors of the HMMPE blends were also characterized by a capillary rheometer (CR) (Göttfert Rheograph 2003A, Germany) at 190 °C and 230 °C. Here, the controlled piston speed mode was used with the round hole capillary dies (nominal L/D ratio equal to 30/1 and die entrance angle 180°). The real die diameters used here were recalibrated before use (Calibrated dies diameters $D = 0.924$ mm and 0.542 mm for the nominal $D = 1.0$ and 0.7 mm dies).

2.2.6. Scanning electron microscopy & transmission electron microscopy

The TC3 white film embedded in epoxy was ultra-microtomed with glass knives on an ultracut microtome (Leica ultracut-R ultramicrotomed, Germany) at room temperature to give sections with a nominal thickness of 75 nm. Transmission electron microscopy (TEM) images were obtained with a transmission electron microscope at 200 kV (JEOL 2010, Japan).

The morphology of the extrudates generated during the capillary rheometric experiment was examined by high resolution scanning electron microscopy (SEM) (JEOL 6700F, Japan) with the acceleration voltage 5 kv. All samples were sputter-coated with a ~200 Å layer of gold to minimize charging. The samples were quenched by compressed air from a hose placed near the die exit, providing a cooling ring. This 'froze' the structure of the TLCP droplets or fibrils before they could relax completely. Micrographs of the surfaces of these samples were taken after etching with a 10 wt% aqueous sodium hydroxide solution at 75 °C for 30 minutes.

The extrudate embedded in epoxy was ultra-microtomed with glass knives on an ultracut microtome at room temperature to produce sections with a nominal thickness of 100 nm. The sections were transferred to Cu grids. To enhance the phase contrast, the sections were stained with a ruthenium tetroxide vapor for 2 hrs. TEM images were obtained with a transmission electron microscope at 200 KV (JEOL 2010, Japan). The 'frozen' extrudate for SEM was used for ultra-microtome. All images were obtained from sample sections microtomed along the flow direction.

3. Results and discussion

3.1. Dispersion and morphology of organoclay

The structures or morphologies of polymer-layered silicate nanocomposites depend on interaction of the polymer with the layered silicate and the dispersion of layered silicate in the polymer matrix. WAXD is a useful and simple measurement to characterize clay morphologies in nanocomposites. The (001) plane diffraction peak observed in the WAXD pattern of TC3 white disappeared, compared with the pattern of layered silicate having d-spacing 2.35 nm, as shown in Figure 1. The clay dispersion in the polymeric matrix was

further examined using TEM. Typical TEM photographs for the TC3 white nanocomposite are shown in Figure 2. The dark plates, 15-25 nm in length, are the organoclays with surfaces paralleling the observed plane. The organoclays were fully exfoliated and well dispersed in the TLCP matrix without any agglomeration.

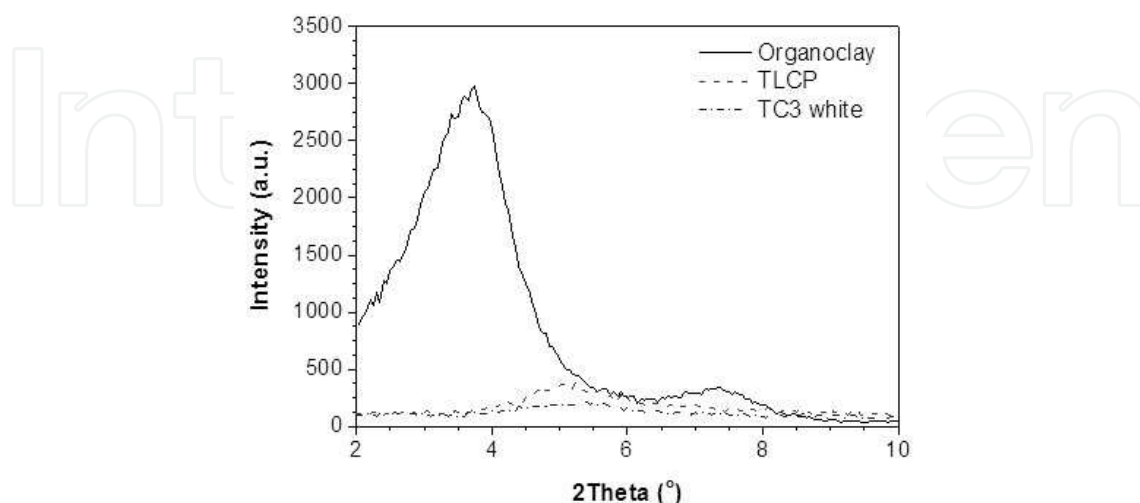


Figure 1. WAXRD patterns of organoclay, TLCP and TC3 white at room temperature.

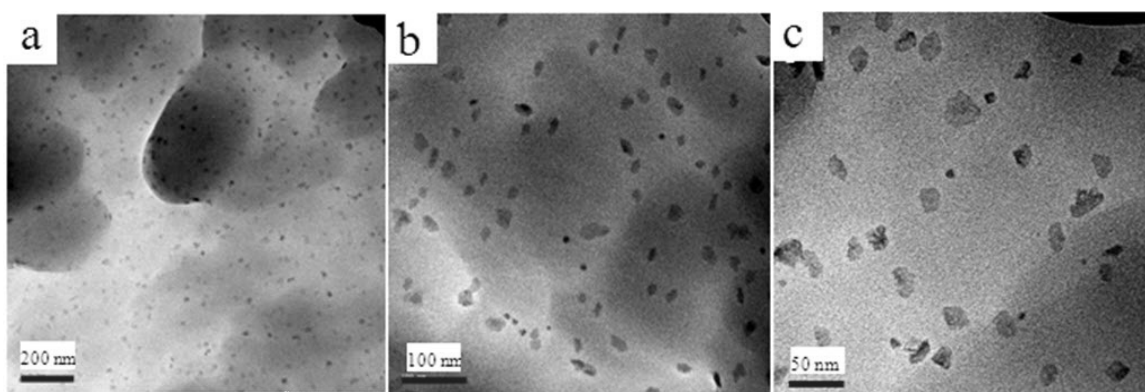


Figure 2. TC3 white TEM micrographs.

3.2. Molecular interactions in nanocomposite

IR spectroscopy is very sensitive to polymer microstructure and has been widely used in the investigation of hydrogen bonding, macromolecular orientation and crystallinity in polymer materials. FTIR with liquid cell was used with chloroform as background. Figure 3 shows the FTIR spectra for chloroform solutions with TLCP and TC3 white under ultrasonic irradiation at room temperature. It can be seen that the peak at the wavenumber of 1060 cm^{-1} in TLCP shifts to the wavenumber of 1045 cm^{-1} in TC3 white. The absorption peak at 1060 cm^{-1} is believed to represent -C-O- in the TLCP molecules. The peak shift is the result of weak interaction between the positively charged N^+ ion in the surfactant 2M2HT residing on the surface of the organoclay Cloisite 20A with -C-O- group in the TLCP molecules.

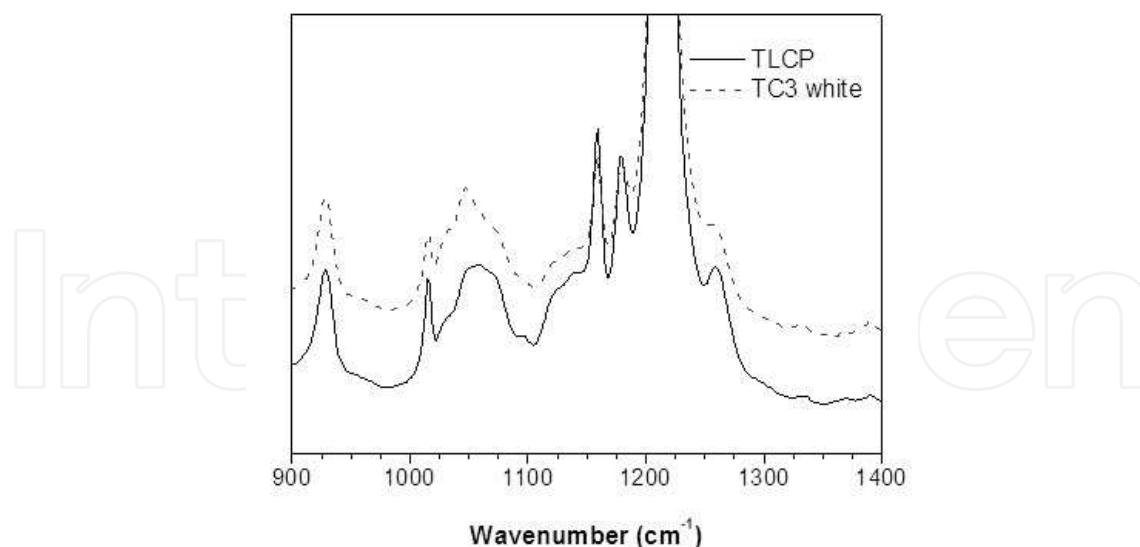


Figure 3. FTIR of TLCP and TC3 white chloroform at room temperature with liquid cell.

Figure 4 shows ^{13}C NMR spectra obtained from TLCP and TC3 white at room temperature. It is well known that a chemical shift between 0-40 ppm corresponds to $-\text{C}-\text{C}-$ coupling. After careful analysis of these regions, it was determined that the peaks at 25.2, 29.4 and 34.7 ppm shown in Figure 4(a), 4(b) and 4(c) belong to the spacer $-(\text{CH}_2)_8-$ in TLCP. No chemical shift occurred but the peaks width increased after addition of the organoclay. The relatively broad peaks are probably due to the shielding effects of the layered silicate gallery on the alkyl chains.

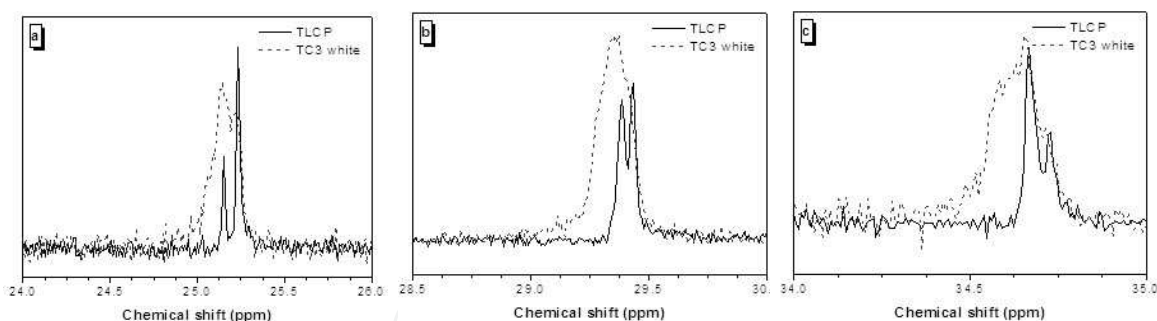


Figure 4. ^{13}C NMR spectroscopies of TLCP and TC3 white in CDCl_3 at room temperature.

3.3. Liquid crystalline mesophase

Figure 5 displays the in-situ microstructure evolution of TLCP and TC3 white using polarization transmission optical microscopy. The incident polarization was oriented along the flow direction and the analyzer was oriented perpendicular to this polarization. The first images are the microstructures of the melted TLCP (Figure 5 (a)) and TC3 white (Figure 5(b)) in the quiescent state at 185 °C. The TLCP micrograph shows textures surrounding different colors (blue, yellow and pink) regions, which indicate domains of different orientations. Compared with TLCP, TC3 white shows the domains (mainly darker yellow)

with few other colors because of the lower light intensity. Upon startup of the shear flow, the domain textures became deformed, stretched and aligned along the shear direction. A gradual increase in the light intensity was observed. During shearing, TLCP (in Figure 5(c)) exhibited colorful textures (yellow, red and blue with some dark areas). TC3 white (Figure 5(d)) exhibited a mainly color (yellow with a few blue and red areas). With the polarized light, darkening may result from the structure becoming either completely isotropic or perfectly oriented along the principal axes. However, the darkening was not observed without the use of a polarizer; therefore isotropy can be ruled out as the primary cause for this darkening phenomenon.

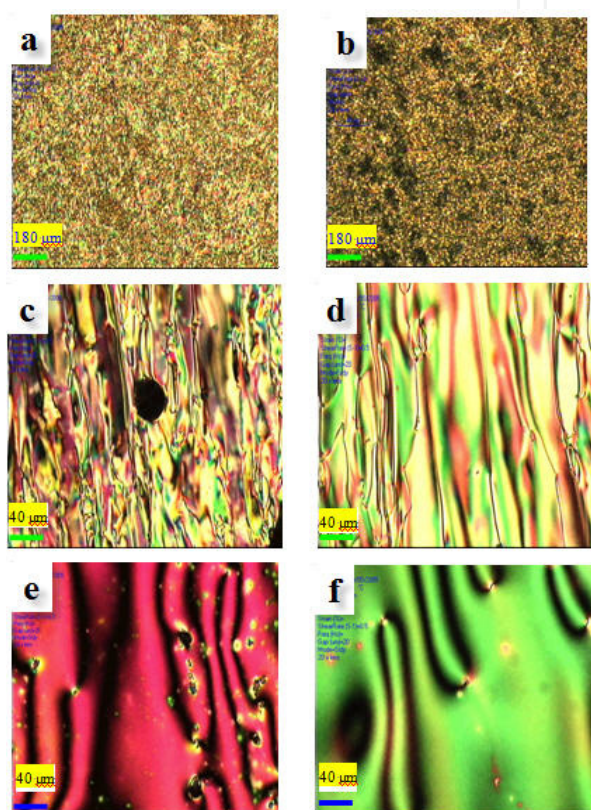


Figure 5. POM images of TLCP (a, c, e) and TC3 white (b, d, f) at 185 °C (a) and (b) before steady shear (X4); (c) and (d) during steady shear at 0.5 1/s (X20); (e) and (f) after steady shear and relax to steady state (X20).

The microstructures relaxation after the flow cessation is illustrated in Figure 5 (e) and 5(f). Once a steady flow was reached, a monodomain with a few defect structures was formed. After the same shear history, TLCP and TC3 white showed different colors. The areas of high Frank elasticity around the $\pm 1/2$ strength defects showed the highest and lowest retardation colors, whereas the bulk of the texture showed an intermediate retardation color. The static texture of the nanocomposite after steady shear is similar to that of the homopolymer. The existence of the fully exfoliated organoclays did not affect the mesophase structure of the TLCP molecules, which may be due to the good dispersion of organoclays and their small sizes.

3.4. Thermal properties

The thermal stability of polymeric material is usually studied by thermogravimetric analysis. Generally, the incorporation of clay into the polymer matrix is found to enhance thermal stability, as the clay acts as a superior insulator and mass transport barrier to oxygen during oxidation in the air condition.

The TGA curves of clay, TLCP, and TC3 white in the air flow condition are shown in Figure 6. No weight loss occurred below 200 °C in any of the samples. Because of the presence of some organic molecules in interlayer spaces, the clay began to lose weight at 230 °C; at 600 °C, the clay weight loss was 30 %, similar to the result reported by Chiu et al. [23] Comparing TLCP with TC3 white, the thermal stability of TC3 white increased. For example, for TLCP, the temperature at which the weight loss started was 335 °C whereas for TC3 white, it was 349 °C. For TLCP, the temperature at which the weight loss was halved was 530 °C and for the nanocomposite, it was 549 °C.

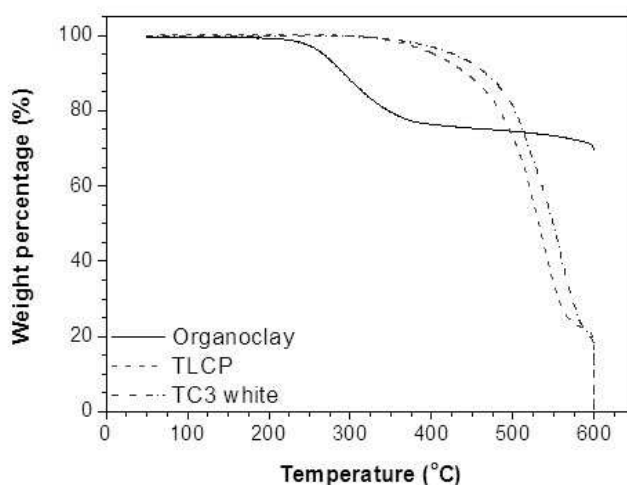


Figure 6. TGA of organoclay, TLCP and TC3 white in air.

TLCP used here was a semicrystalline nematic forming TLCP. From the DSC results, as shown in Figure 7(a), the endothermic peak appearing at ~ 125.5 °C represented the glass transition temperature of TLCP. Due to the broad sequential distribution of the HBA and SA-HQ segments in TLCP [24], two broad endothermic peaks at ~152 °C and ~164 °C represented the melting temperatures of the crystalline phase of TLCP with different segments. With the introduction of the well-dispersed nanoclay into the system, the glass transition temperature shifted to a higher temperature, peaking at ~ 142 °C, and the two melting temperatures peaked at ~ 159 °C and ~ 167 °C. The exothermic peaks are exhibited in Figure 7(b). The exothermic peak positions also changed and became sharper with the introduction of clay. For TLCP, there were two peaks, at ~166 °C and ~159 °C, corresponding to the different crystalline peaks with different molecular chain lengths as shown. With the introduction of the exfoliated layered silicates, the sharp exothermic peak was followed by a broad peak in the nanocomposite at corresponding temperatures of 163.5 °C and 169 °C respectively. With the effect of the layered structure, the arrangement of liquid-crystalline

polymer chains became more ordered. There is no doubt that the transition temperatures in the heating and cooling curves increased in TC3 white.

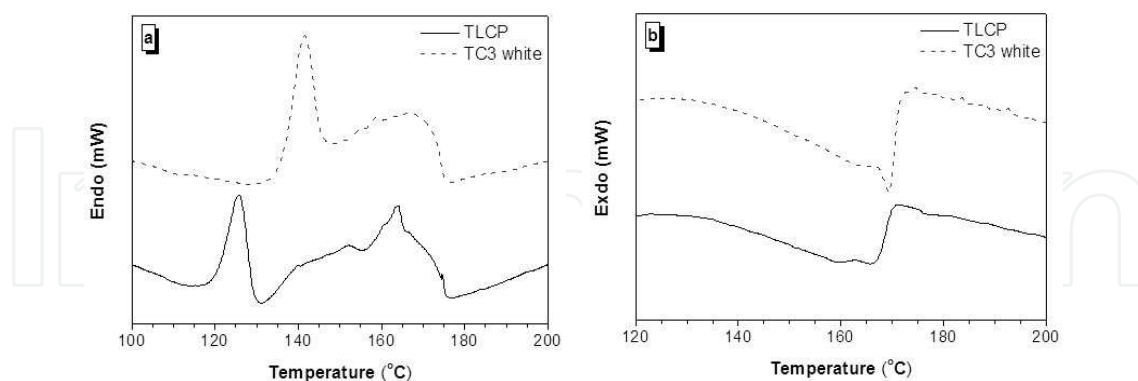


Figure 7. Second heating (a) and cooling (b) curves of TLCP and TC3 white at N₂ atmosphere.

3.5. Rheological properties

3.5.1. Organoclay modified TLCP nanocomposite

Linear viscoelasticity

Dynamic frequency sweeps at strains well within the linear viscoelastic regime of each material were performed in a range of frequencies covering 5 decades (0.01 – 1000 rad/s). The results shown in Figure 8 exhibit the storage modulus G' , loss modulus G'' and complex viscosity η^* for TLCP and TC3 white. For TLCP, G' , G'' and η^* became too small and scattered for accurate measurement at lower frequencies (in the region of 0.04 rad/s to 0.25 rad/s). This was due to the low viscosity of the melt at 185 °C, which led to torque values beyond the limits of the transducer. In the low frequency region (0.04 rad/s to 0.25 rad/s), TC3 white had dependable data but the TLCP data was scattered. In this region, slopes for G' and G'' were 0.12 and 0.31 for TC3 white, and 0.30 and 0.55 for TLCP. The corresponding slope values for η^* were 0.83 and 0.58. Pseudo-solidlike behaviors existed in TLCP and TC3 white, with TC3 white exhibiting more solidlike behavior than TLCP. The polydomain structure in the bulk state of TLCP is the reason for TLCP behavior [25]. The percolated network formed by the exfoliated organoclay with the TLCP molecules enhanced those polydomain structures, causing more solidlike behavior and higher η^* in the lower frequency region in TC3 white. In the middle frequency region, both showed plateaus of nearly constant viscosity. The TC3 white curve paralleled the x-axis and TLCP had a small slope value of -0.15. At high frequencies, TC3 white showed a gradual change of slope to -0.21, whereas TLCP maintained the same slope. In this region, the slopes of G' and G'' for TLCP were 0.70 and 0.86 but for TC3 white, they were 1.83 and 0.92. There were dramatic differences between the two materials. The slopes for TC3 white approached the theoretical values for polymers with flexible chains, which are 2 and 1, respectively. With the help of exfoliated clay in high frequencies, TC3 white performed like flexible chains, whereas TLCP still showed some entanglement behavior.

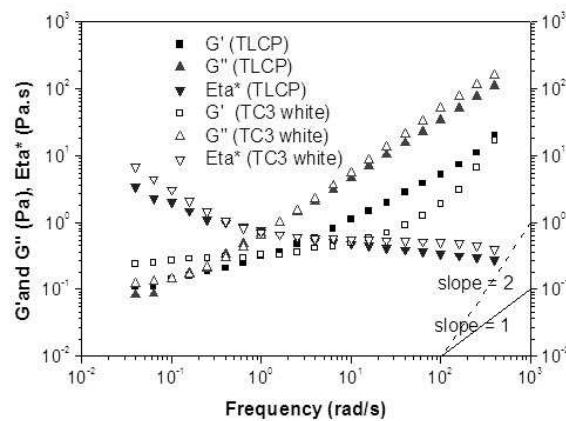


Figure 8. Storage modulus G' , loss modulus G'' and complex viscosity Eta^* in dynamic frequency sweep for TLCP and TC3 white at 185 °C.

It has been claimed that the Cole-Cole plot of storage modulus vs. loss modulus can provide information about structures. The Cole-Cole plot for TLCP and TC3 white is shown in Figure 9. From a log-log plot of G'' vs. G' , we can determine that the slope α in $G' \sim (G'')^\alpha$. For a single Maxwell element, $\alpha = 2$, however, complex systems with associations often deviate from the single element, and this can be seen by an exponent α that deviates from 2. For TLCP, the slope was constant with a value of 0.776 in the whole region, which has a large deviation with flexible chain polymers ($\alpha = 2$). This is due to TLCP intrinsic anisotropic properties. For TC3 white, with the loss modulus increasing, the slope changed dynamically from almost zero (pseudo-percolation behavior or solid-like behavior), gradually approaching the theoretical flexible chain value, 2. This plot showed that there were different structural responses for TC3 white in different frequency regions.

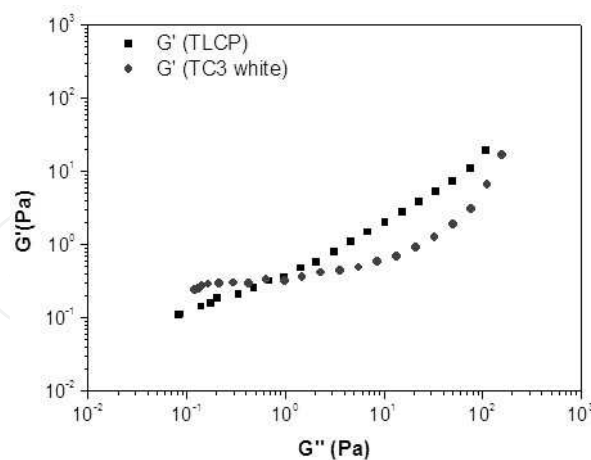


Figure 9. The cole-cole plot of loss modulus G'' vs. storage modulus G' for TLCP and TC3 white at 185 °C.

Cox-Merz rule

Figure 10 provides global view of TLCP and TC3 white viscosities as a function of frequency or steady shear rate. Unlike other organoclay based polymeric nanocomposites, the

measured viscosity of TC3 white is similar to that of the TLCP matrix at the same frequency or shear rate. The curves, especially the TC3 white curve, are reminiscent of the three-region viscosity curve reported by Onogi and Asada [25] for lyotropic polymer. The phenomenon can be explained by polydomain structures. With the addition of the organoclay, the three-region viscosity phenomenon was enhanced. TC3 white performs more like lyotropic polymer, with a more rigid structure than the semi-rigid TLCP. The TC3 white curves fitted the Cox-Merz rule, i.e. $\eta(\dot{\gamma}) = |\eta^*(\omega)|$, where $\dot{\gamma} = \omega$. However, the Cox-Merz rule failed for TLCP, a finding which has also been reported by other researchers [26].

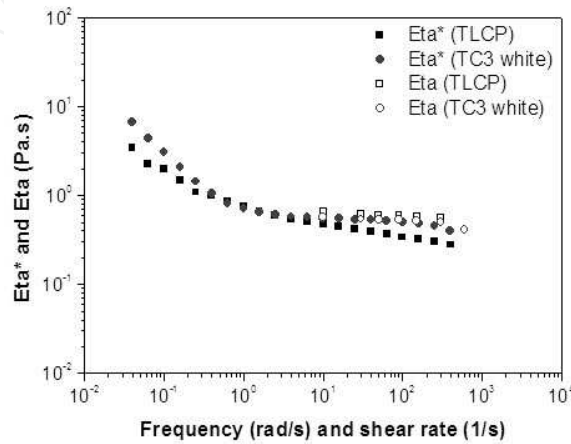


Figure 10. Cox-Merz rule on TLCP and TC3 white at 185 °C.

The first normal stress difference measurement

The cone and plate fixture, with its constant rate of shear and direct measurement of the first normal stress difference N1 by total thrust, is probably the most popular rotational geometry for studying non-Newtonian effects. Figure 11 shows the total thrust (normal force) for TLCP and TC3 white at different shear rates at 185 °C using a 50 mm diameter cone and plate fixture. The normal force evolution at a particular constant shear rate was clearly exhibited with a few peaks (or shoulders) at small strain before reaching a steady state. These peaks corresponded to the structure being broken and aligning during shear [27].

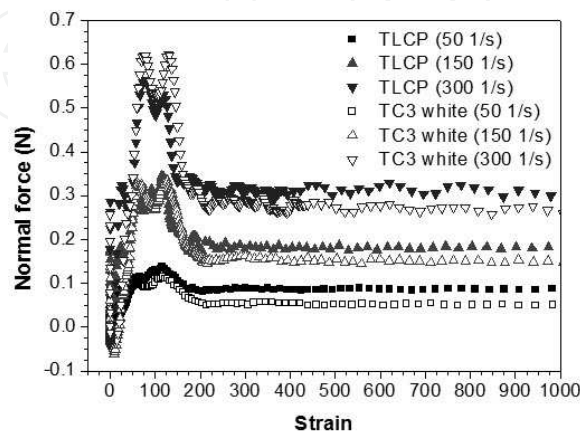


Figure 11. Normal force for TLCP and TC3 white at different shear rates with cone and plate fixture at 185 °C.

For the total thrust data measured in the cone and plate fixture, some equations can be used to calculate the N_1 for TLCP and TC3 white [28].

For the cone and plate fixture:

$$N_1 = \frac{2F_z}{\pi R^2} \quad (1)$$

Where, F_z is the total thrust measured in the cone and plate fixture. R is the radius of the cone and plate fixture.

Due to the inertia and secondary flow effect, i.e. in cone and plate rheometers, inertia forces tend to pull the plates together rather than push them apart, a corrected term must be introduced to eliminate this effect:

$$(F_z)_{inert} = 0.075\pi\rho\Omega^2R^4 \quad (2)$$

Where, ρ is the density of the material, Ω is the angular rotation rate.

After this correction the N_1 can be calculated:

$$N_1 = \frac{2F_z}{\pi R^2} - 0.15\rho\Omega^2R^2 \quad (3)$$

The steady state N_1 at different shear rates at 185 °C can then be calculated. The graph is shown in Figure 12. Due to the low viscosity, the maximum shear rate that could be measured was 300 1/s for TLCP and 600 1/s for TC3 white. The sample spun out with a dramatic and continuous decrease in stress and viscosity when the shear rate was larger than the above value. In Figure 12, N_1 s are positive for TLCP and TC3 white with comparable values.

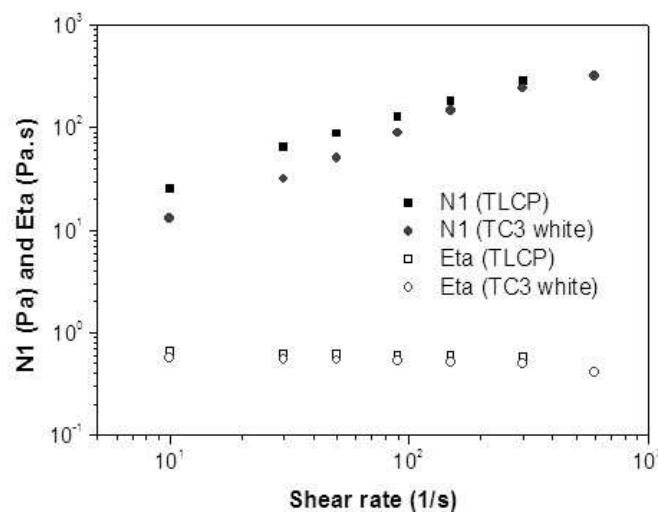


Figure 12. Shear rate dependence of shear viscosity η and first normal stress difference N_1 for TLCP and TC3 white at 185 °C.

For N1, molecular theory, especially the Doi theory (for rod-like nematics) [29] predicts that the director (or local average orientation) will rotate or tumble with the flow. At low shear rates, N1 will be positive. At intermediate rates (when the flow rate is a little slower than the reciprocal of the longest molecular relaxation time), nonlinear effects are important, producing competition between tumbling and steady alignment of the director along the flow. As a result, the director oscillates about a steady value [30]. In this “wagging” regime, which is peculiar to tumbling, polymeric nematics and the local molecular order are significantly weakened, and N1 is negative. At very high rates of shear, the director aligns in the flow direction, and N1 is again positive. The Doi molecular theory for rod-like nematics was remarkably applicable with experimental data for PBG solutions [31]. Although a similar coupling between flow and liquid-crystalline order is conceivable in thermotropics, experiments have not yielded a corresponding agreement with theory. In fact, the expected pattern of sign changes in N1 has not been observed [32]. The N1 curves in Figure 12 for these two systems are in the high-shear-rate region, with $N1 > 0$. Figure 12 displays the shear rate dependence of η and N1 for TLCP and TC3 white at 185 °C. From comparison of the N1 values between TLCP and TC3 white, it can be observed that the values of N1 for TC3 white are a little lower than those for TLCP, but the rate of the N1 increase in TC3 white is higher. Combined with the viscosity variations with shear rate, these phenomena indicate that the presence of exfoliated clay increases elasticity in a flow-aligning state, and the exfoliated clay is oriented along the shear direction, even assisting the neighboring TLCP molecules to align in the flow direction, with the result that there is a decrease of viscosity and an increase of N1 slope, as shown in Figure 12.

The dispersion of the exfoliated clay in the TLCP matrix without and with deformation is depicted schematically in Figure 13(a) and 13(b), respectively, where the dark ellipses represent clay platelets, the wavy lines and cylinders represent TLCP chains with flexible and rigid components, and the short dashed lines represent the interaction between TLCP and clay. It should be noted that in the conformation of TLCP, the phenyls in HBA and HQ are not coplanar, and hence the SA flexible segments connected to the HQ are not in a line with HBA. In the schematic diagram, the effect of the exfoliated clay on TLCP is clearly delineated. Without deformation (Figure 13(a)), the disordered dispersion of the exfoliated clays in the TLCP matrix is presented. On the other hand, with deformation (Figure 13(b)), shear-induced molecular alignment in both TLCP and TC3 white occurs along the shear direction.

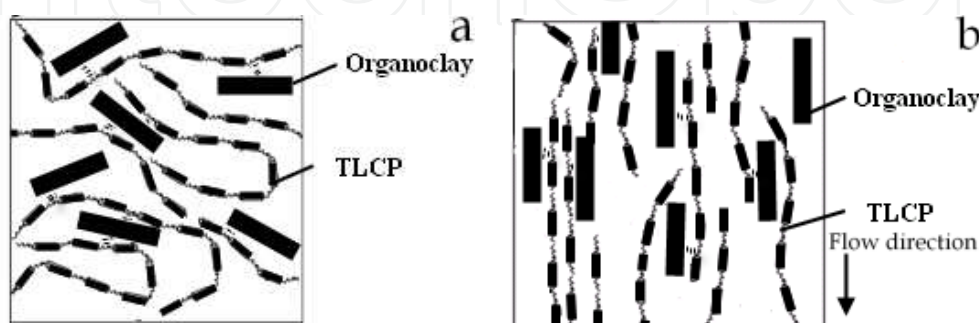


Figure 13. Schematic drawing of TLCP molecular chains influenced by the exfoliated organoclays (a) without and (b) with deformation.

3.5.2. High molecular mass polyethylene blends

Shear deformation

The linear viscoelasticity and large amplitude stress relaxation tests were performed by an ARES at 190 °C. Complex viscosities in frequency sweep and stress relaxation modulus with strain 300.0 % are exhibited in Figure 14(a) and (b) separately. In Figure 14(a), little difference is shown between the curves, indicating that the purified TLCP and TC3 white had little influence on the HMMPE matrix in the linear viscoelastic region. Large amplitude stress relaxation tests were performed in the nonlinear region. The curves in Figure 14(b) show no difference over the entire relaxation periods. All the information demonstrates that the purified TLCP and TC3 white had little effect on the shear deformation of the HMMPE at the above particular conditions.

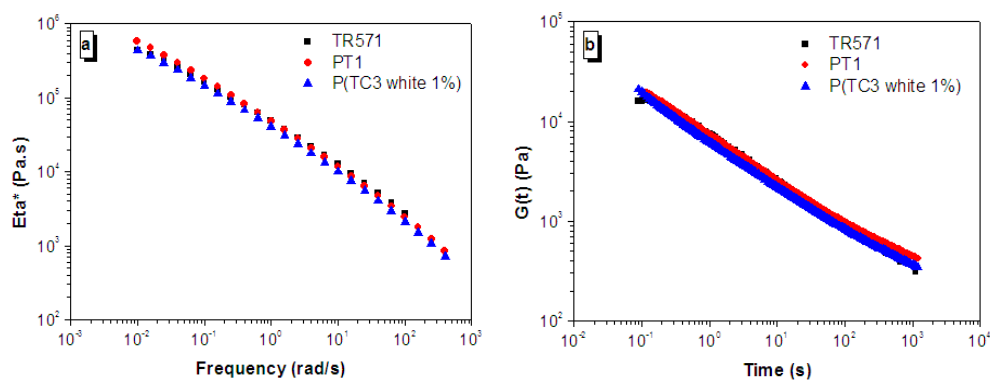


Figure 14. (a) Dynamic frequency sweep and (b) stress relaxation in nonlinear region with strain = 300.0 % of HMMPE [TR571], HMMPE/TLCP 1.0 wt% [PT1] and HMMPE/(TC3 white 1.0 wt %) [P(TC3 white 1%)] at 190 °C.

Elongation deformation

The effects of purified TLCP and TC3 white on the HMMPE matrix were also characterized using a pressure-driven rheometer. Here, the controlled piston speed mode with the round hole capillary dies at 190 °C and 230 °C was used. Capillary flows are usually considered as simple shear flows. The shear stress is highest near the capillary die wall, where the polymer chains are most likely to be stretched to an extended configuration. This is valid only if the melt shows negligible entrance effects. Entrance effects are caused by the elongational flow due to the converging melt flowing from the reservoir into the capillary die with large contraction ratios. The polymer melt along the centerline will experience the highest stretching rate. It has been observed that such effects are extremely important when anisotropic melts such as TLCPs are studied.

Rheological behavior at 190 °C.

Apparent shear viscosities as a function of shear stress at wall for HMMPE [TR571], HMMPE/(purified TLCP 1.0 wt%) [PT1] and HMMPE/(TC3 white 1.0 wt %) [P(TC3 white 1%)] with the same L/D ratio (30) and different diameters (0.7 mm and 1.0 m) at 190 °C are

shown in Figure 15. At this temperature, TLCP shows the nematic structures [20]. Significant viscosity reductions are initially observed in different die diameter tests. Based on an equivalent wall stress of 10^5 Pa , the viscosity reductions at 190°C with $L = 21 \text{ mm}$ and die radius equal to 0.271 mm for the different blends are: for PT1, a similar viscosity to that of HMMPE, because no yielding occurred; for P(TC3 white 1%), 98.5 % viscosity reduction compared to HMMPE (corresponding apparent shear rate 317.6 1/s). For the maximum processing rate, HMMPE is $\sim 39 \text{ 1/s}$, PT1 is $\sim 318 \text{ 1/s}$, whereas P(TC3 white 1%) is up to $\sim 700 \text{ 1/s}$. P(TC3 white 1%) can achieve a shear rate almost 20 times higher than that of HMMPE and twice as high as that of PT1.

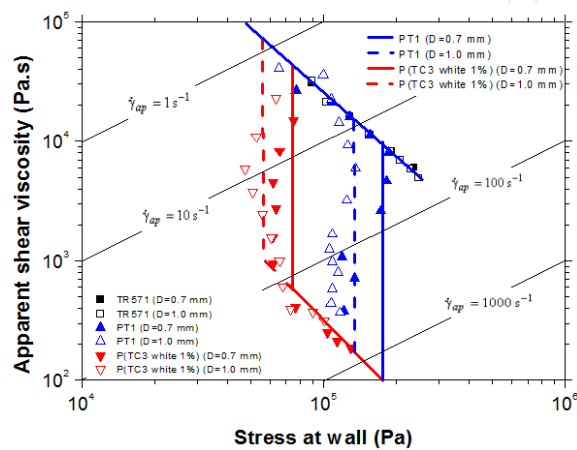


Figure 15. Apparent shear viscosities as a function of shear stress at wall for HMMPE [TR571], HMMPE/TLCP 1.0 wt% [PT1] and HMMPE/(TC3 white 1.0 wt %) [P(TC3 white 1%)] with the same L/D ratio (30) and different diameters (0.7 mm and 1.0 m) at 190°C with capillary rheometer. (The points were measured data and the lines were simulated data).

A yielding-like behavior is shown by all blends when the wall stress is almost constant over a region of rapidly decreasing viscosity. However, yielding stresses and the corresponding beginning and ending apparent shear rates are different for each blend. Table 1 details the yielding behaviors of the blends. From the table, it is clear that with the organoclay modified, much lower values of yielding stress were needed. Moreover, the apparent shear rate of all blends at the beginning of transition is much lower than that of PT1. This explains why it is difficult to obtain the first power-law region in capillary rheometer tests for P(TC3 white 1%) in simulation, as we describe later in this study. Due to the low yield stress and the initial transition shear rate, the blend can easily move through the transition zone and reach the zone with lower viscosity. The low energy input needed to process the blend holds promising potential for industrial application.

Rheological behavior at 230°C

The rheological behaviors of three materials at 230°C are presented with a plot of apparent shear viscosities as a function of shear stress at wall in Figure 16. At this temperature, TLCP shows nematic/isotropic biphasic structures. Based on an equivalent wall stress of 10^5 Pa , for PT1, the yielding stress is higher than 10^5 Pa , and has similar viscosity to that of

HMMPE; for P(TC3 white 1%), a viscosity reduction of > 93% was achieved at 230 °C. The maximum processing shear rates are ~ 66 1/s for HMMPE, ~ 315 1/s for PT1 and ~ 904 1/s for P(TC3 white 1%). Table 2 lists the experimental data for yielding stress and transition shear rates for the blends at 230 °C. Similar with the parameters at 190 °C, lower yielding stresses are obtained in PT1 and P(TC3 white 1%). A more obvious phenomenon concerns the transition zone, which is narrow in the range of 8 1/s to 23 1/s for P(TC3 white 1%) and still cannot obtain transition ending shear rate for PT1. A small force can be used to pass through the narrow transition zone to arrive at the low viscosity region at this temperature for P(TC3 white 1%).

Yielding behaviors	Stress (Pa)		Beginning $\dot{\gamma}_{ap}$ (1/s)		Ending $\dot{\gamma}_{ap}$ (1/s)	
	0.7	1.0	0.7	1.0	0.7	1.0
PT1	1.63 × 10 ⁵	1.34 × 10 ⁵	41.0	24.1	855.8	476.9
	1.61 × 10 ⁵	1.36 × 10 ⁵	39.8	22.9	---	---
P(TC3 white 1%)	7.22 × 10 ⁵	5.78 × 10 ⁵	5.6	3.3	215.7	120.1
	7.08 × 10 ⁵	5.90 × 10 ⁵	6.0	3.5	207.4	110.8

Table 1. Typical parameters with experimental and simulated tests for HMMPE blends at 190 °C (Bold data are predicted results).

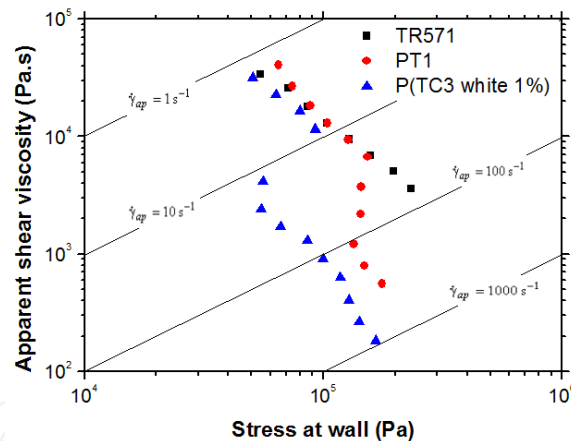


Figure 16. Apparent shear viscosities as a function of shear stress at wall for HMMPE [TR571], HMMPE/TLCP 1.0 wt% [PT1] and HMMPE/(TC3 white 1.0 wt %) [P(TC3 white 1%)] with L/D ratio = 30 and diameter = 1.0 mm at 230 °C with capillary rheometer.

The yielding-like behavior in P(TC3 white 1%) presents an obvious negative gradient. We suggest that the negative gradient is due to TLCP phase transition in the TLCP/organoclay hybrid from isotropic to nematic, or maintaining the isotropic phase at that temperature. TLCPs are known and theoretically understood to undergo shear-induced phase transitions when the domain orientation is sufficient high [33, 34]. Chan et al. [2] have presented the results of optical microscopy/shearing experiments demonstrating a phase transition from isotropic to nematic for this type of TLCP. A pre-translational order in the isotropic phase of a homologous series of liquid crystals close to the isotropic-to-nematic transition has also been

experimentally observed. De Schrijver et al. [35] used a transmission ellipsometric technique to observe this surface-induced isotropic ordering. For the P(TC3 white 1%) blend, since fully exfoliated organoclay structures were formed in the TLCP, no confinement existed to hold an ordered structure and cause phase transition, but there were interactions, such as long-range non-bond forces, which also gave structures more order and retained the orientation even during the relaxation period [22].

Yielding behaviors	Stress (Pa)	Beginning $\dot{\gamma}_{ap}$ (1/s)	Ending $\dot{\gamma}_{ap}$ (1/s)
PT1	1.27×10^5	13.6	---
P (TC3 white 1%)	0.56×10^5	8.0	22.9

Table 2. Typical parameters with experimental tests for HMMPE blends at 230 °C.

3.6. Morphological studies

The SEM diagrams of etched extrudates are shown in Figure 17 with magnification 20,000. For the HMMPE, as shown in Figure 17(a), the etched strand gives a rough and highly topological contrast. Moreover, a fine line texture is disclosed after NaOH etching. This indicates that some surface materials or even layers are removed during the etching process. PE is a material that strongly resists attack by NaOH. Therefore, the detached material is thought not to be pure PE. It would be too difficult for NaOH to diffuse into the PE lattice and remove it from the surface. As has already been illustrated by Chan et al. [36] the material removed is an anti-oxidant enrich polyethylene layer, which is caused by migration of anti-oxidant during shear. The surfaces of the blends are smooth at those apparent shear rates. At higher magnification, some interesting features are revealed. Long and thin cavities are seen, with the long dimension paralleling to the flow direction. These cavities are due to the removal of TLCP filaments. In these well defined morphologies: a PT1 strand (Figure 17(b)) shows only fibrillar structures aligned along the flow direction; also within a P(TC3 white 1%) strand (Figure 17(c)) only longitudinal fibrillar striations exist. Both images show that in situ fibril formation occurs during elongation in both blends.

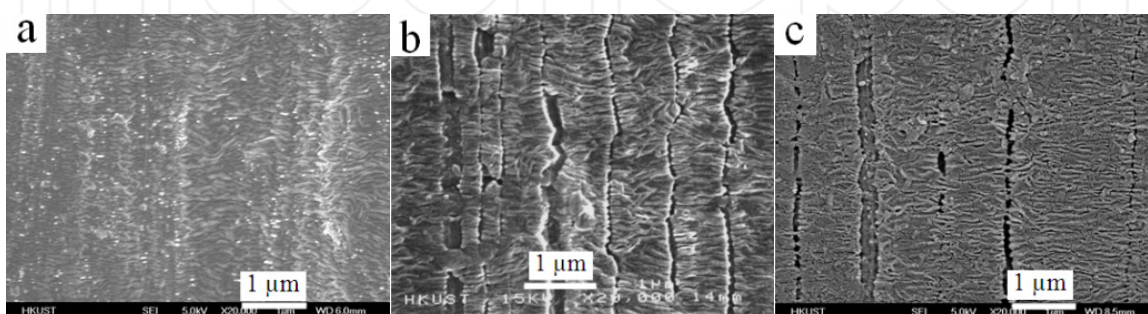


Figure 17. SEM images of (a) HMMPE [TR571], (b) HMMPE/TLCP 1.0 wt% [PT1] and (c) HMMPE/(TC3 white 1.0 wt %) [P(TC3 white 1%)] with magnification 20,000X.

TEM images of P(TC3 white 1%) are exhibited in Figure 18 with different magnifications. Global alignment of PE lamellae can be clearly seen in Figure 18(a), with typical row-nucleated shish-kebab structures (a schematic drawing in the insert of Figure 18(a)), a structure which is usually observed when PE crystallization takes place under stress [37, 38]. The long fiber crystals formed by the extended high molecular mass fractions act as nucleation sites for the growth of folded PE crystals. Detail micrographs (Figure 18(b) and 5(c)) clearly show the strong interfacial compatibilities between the aligned TC3 white filament and the adjacent PE matrix. Also the embedded TC3 white fiber exhibits a regular banded structure, all the bands being perpendicular to the direction of chain alignment. The above observations are similar to those in our earlier studies of PT1 systems [39], indicating that they have a similar viscosity reduction mechanism [40].

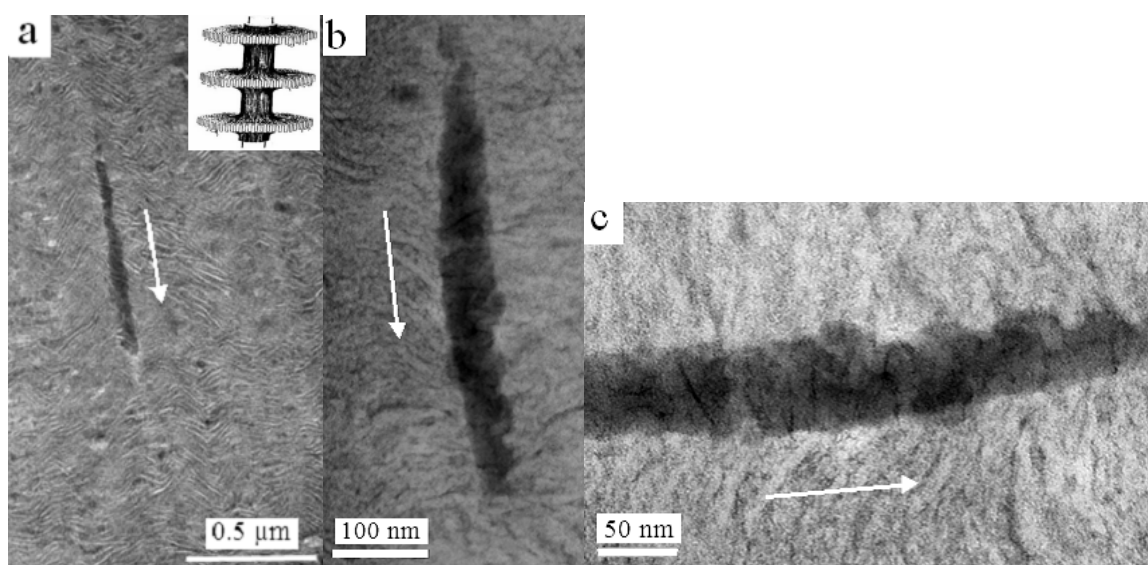


Figure 18. TEM micrographs of the lateral section of the HMMPE/ (TC3 white 1.0 wt %) [P(TC3 white 1%)] blend extrudate surface prepared parallel to the flow direction at different magnifications.

3.7. Texture studies

The textures of purified TLCP and TC3 white at 230 °C and 250 °C are presented in Figure 19 with different magnifications. These samples all underwent the same thermal history with the following steps: (1) sheared at shear rate 0.5 1/s for 3600 seconds at 185 °C; (2) maintained at this temperature to obtain stable texture; (3) temperature ramped to 230 °C at 5.0 °C/min; (4) obtained texture structure after structure evolution for a specified period. From previous results [22] the purified TLCP and TC3 white displayed a similar texture after steps (1) and (2) at 185 °C. The fully exfoliated organoclay did not affect the liquid crystallinity and mesophase structure at the nematic state at 185 °C. In Figure 19(a) and (b), an isotropic phase is clearly presented alongside the nematic phase after steady shear at 0.5 1/s for 600 seconds at 230 °C and relaxation for 600 seconds for purified TLCP. The nematic phase exists in dispersed and discrete regions containing defect lines, which are highly birefringent and contain domains of anisotropy. The isotropic phase is continuous. There is a distinctly biphasic, nematic/isotropic, texture in purified TLCP at 230 °C. With the elapse

of time, a spherical shaped nematic region with a more relaxed state (indicated by the presence of fewer line defects inside the sphere) occurs. Figure 19(c) presents an image of purified TLCP after shearing at 5.0 1/s for 60 seconds followed by relaxation for 600 seconds at 230 °C. The area of continuous isotropic phase has become larger than the nematic phase. With increased of temperature to 250 °C, as Figure 19(d) shows, the nematic phase gradually diminishes in size and population within the isotropic phase matrix. For TC3 white, as shown in Figure 19(e) and (f), after steady shearing at 0.5 1/s for 600 seconds followed by relaxation for 600 seconds, a dominant nematic texture occurs with few dispersed isotropic regions at 230 °C. The defects which were stable at 185 °C become unstable at 230 °C, due to the effect of the high temperature. As time elapses, the isotropic phase occurs in a minority of discrete regions, and the nematic phase is still dominant. Even after steady shearing at a high shear rate 5.0 1/s for 60 seconds followed by relaxation for 600 seconds at 230 °C, the nematic phase still exists as a continuous structure with a few discrete isotropic structures, as shown in Figure 19(g). The exfoliated organoclays enhance the rigidity of the TLCP molecules and keep them in ordered structures at the high temperature. The competition between the high thermal energy and the internal molecular interactions of the organoclay and TLCP molecules causes the nematic phase to be dominated by biphasic structures for TC3 white at 230 °C. Even at a higher temperature, i.e. 250 °C, after 5.0 1/s shearing for 60 seconds followed by relaxation for 300 seconds, the nematic phase is still in continuous mode, as Figure 19(h) shows.

For the organoclay-modified TLCP, i. e. TC3 white, the combination of the above mentioned nematic dominated structure and shear-induced isotropic-nematic transition had the effect that its rheological behavior at 230 °C was similar to that at 190 °C, with even a higher processing window and a lower transition region.

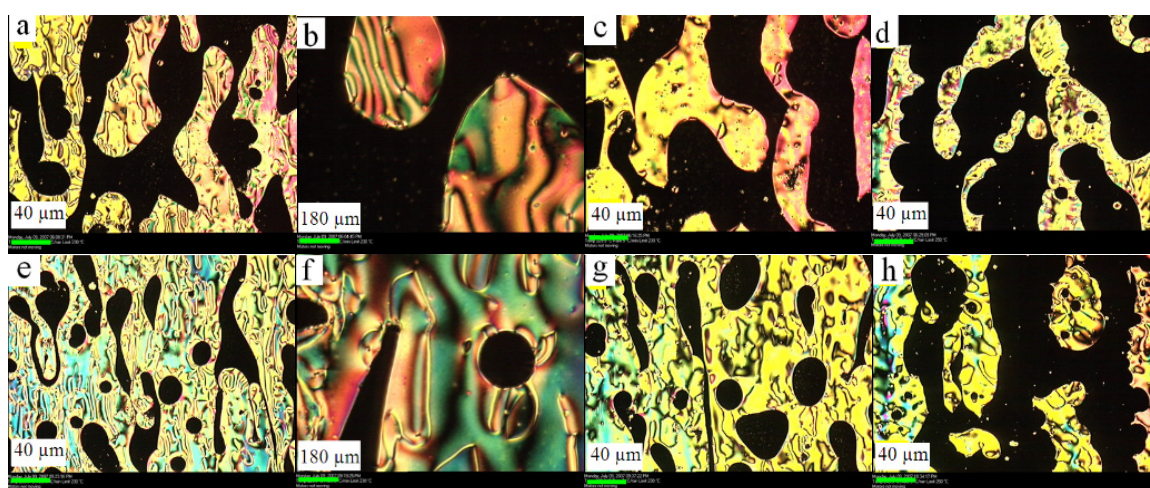


Figure 19. Polarized optical microscope images of (a)(b) purified TLCP and (e)(f) TC3 white relaxed for 600 seconds at 230 °C after steady shear with 0.5 1/s for 600 seconds; (c)purified TLCP and (g) TC3 white relaxed for 600 seconds at 230 °C after steady shear with 5.0 1/s for 60 seconds; (d)purified TLCP and (h) TC3 white relaxed for 300 seconds at 250 °C after steady shear with 5.0 1/s for 60 seconds (all samples have been sheared with shear rate 0.5 1/s for 3600 seconds and relaxed to steady state at 185 °C).

4. Predictions based on a phenomenological model

A binary flow pattern model, previously used for prediction of the effects of a small amount of TLCP in HMMPE (TR570) [40] was used to simulate the rheological responses of the blends in this study.

4.1. Model

To account for the structural effects due to elongational flow along the centerline region in the capillary die, the overall melt flow characteristics are divided into three regions depending on the magnitude of the maximum fluid velocity in the capillary that is usually along the centerline in converging flows. This critical fluid velocity corresponds to the maximum stretching rate of the TLCP (or TC3 white) domains at which irreversible TLCP (or TC3 white) domain elongation into slender filament occurs. The three regimes are:

Region I: The fluid velocity is below the critical velocity for irreversible TLCP (or TC3 white) domain elongation, and the flow of the blends is dominated by the melt flow behavior of the matrix polymer HMMPE melt, independent of TLCP (or TC3 white). A schematic illustration of the melt structure during flow in Region I is shown in Figure 20(a). PE chains formed random coiled conformation and TLCP (or TC3 white) has ellipse shapes with uniform dispersion in PE matrix. The insert in Figure 20(a) shows the organoclay and TLCP chain conformation at this region. Organoclays of uniform size were well and irregularly dispersed in the nematic phase TLCP.

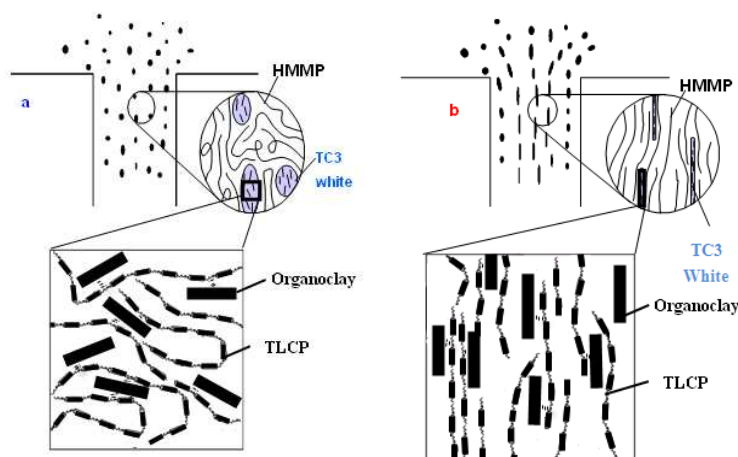


Figure 20. Schematic drawing of HMMPE chains, TLCP chains and organoclay morphological change in capillary die at 190 °C (a) before and (b) after critical shear rates.

Region II: The maximum fluid velocity within the capillary reaches the critical velocity at the entrance of the capillary and irreversible elongational deformation of the TLCP (or TC3 white) domains into long slender fibrous forms begin to occur. This causes a rapid chain elongation and disengagement in the PE melt adjacent to the TLCP (or TC3 white) domains. Consequently, a region of low viscosity melt is formed in the center core of the capillary die.

This center region expands as the flow rate increases until all fluid within the capillary is filled with such melt. The simulated velocity profile developments of fluid flowing through a capillary die to describe the above phenomenon will be presented later in this study. A schematic illustration of the melt structure during flow in Region II is shown in Figure 20(b). The insert in Figure 20(b) shows the chain conformations of TLCP molecules with help of organoclay. Shear-induced molecular alignment occurs with TLCP molecules and organoclay oriented along the elongation direction.

Region III: After all low viscosity fluid is formed across the entire capillary die diameter, a homogeneous melt flow corresponding to the low viscosity melt may be assumed again.

4.2. Velocity profiles

The velocity profile developments of fluid flowing through capillary dies are shown in Figure 21.

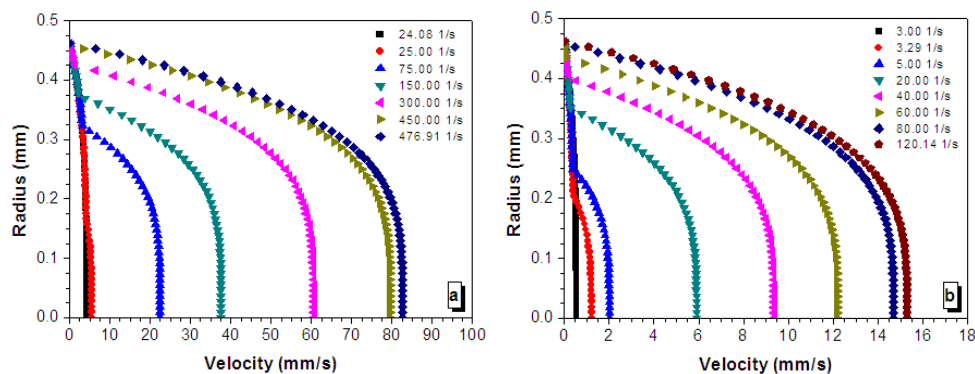


Figure 21. Velocity profile development in region II of flow at $R = 0.462$ mm for (a) HMMPE/TLCP 1.0 wt% and (b) HMMPE/TC3 white 1.0 wt% at 190 °C by simulation.

As shear rate increases, the center core region characterized by low viscosity melt flow characteristics expands from the center core towards the die wall. Close to the wall, the velocity profiles are independent of apparent shear rates. This implies that the shear rates at the wall are independent of flow rates of fluid during the melt structure transition period. Consequently, the wall shear stresses will remain constant throughout this transition period. In the velocity profiles for the different blends, the real die diameters were used instead of the nominal diameters. For nominal diameters 1.0 mm and 0.7 mm, the real calibrated diameters were 0.924 mm and 0.542 mm. Table 1 shows the predicted yielding stress and transition shear rates with the experimental data. The predicted data coincide well with the experimental results. The prediction results also give the end transition shear rates for PT1 at 190 °C with different die diameters, which cannot be obtained experimentally due to the flow oscillation.

4.3. Flow curves simulation

The flow curves are divided into three regimes as described above. In Regions (I) and (III), simple power-law constitutive relations are assumed. In Region (I), because of the relatively

lower yielding shear rates for these blends, dynamic frequency sweep data performed on ARES were used combined with data from CR for simulation. The flow curves in Region (II) were obtained using the velocity profiles together with the power-law parameters in Regions (I) and (III). Figure 22 shows the schematic drawing of apparent shear viscosity as a function of shear stress at wall at the different stages in capillary die. Precise flow curves with Matlab program simulation for the blends are plotted in Figure 15 together with experimental data. Excellent agreement between the model prediction and the experimentally measured flow curves are obtained.

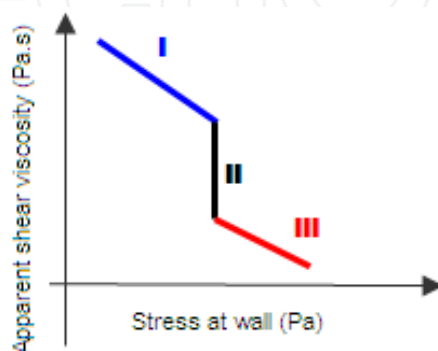


Figure 22. Schematic drawing of apparent shear viscosity evolution as a function of stress at wall at different stages in capillary die at 190 °C.

5. Conclusions

An organoclay-modified TLCP nanocomposite (TC3 white) with the organoclays of uniform size 15-25 nm in length well dispersed in thermotropic liquid crystalline polymer (TLCP) with fully exfoliated structures was designed and prepared by a combination method. Polarized optical microscope images showed that the organoclay did not affect the liquid crystallinity and mesophase structures of the TLCP matrix. However, thermal stability and thermal properties were affected by the organoclay, enhancing the thermal stability of TLCP and shifting the transition temperatures to the high ends. The presence of organoclays caused the nanocomposite to present different rheological behaviours with TLCP at the nematic temperature, i.e. 185 °C. Dynamic experiments demonstrated that TC3 white displayed higher pseudo-solidlike behaviour than TLCP alone in the low frequency region. TC3 white had a similar but even lower viscosity and the first normal stress difference (N1) than TLCP, but the rate of N1 increase in TC3 white was greater than that in TLCP. When enhanced with organoclays, TLCP became more rigid, and with a slight deformation in the TC3 white melt, organoclay helped the TLCP molecules to align in the shear direction and to retain the orientation.

The rheological behaviours of purified TLCP and TC3 white in high molecular mass polyethylene (HMMPE) were characterized by capillary rheometer (CR) with nominal dies of $L/D = 30$ and diameters 0.7 mm and 1.0 mm at 190 °C, where purified TLCP and TC3 white showed similar nematic phase structures. At 230 °C, purified TLCP presented as a continuous isotropic phase with a minority of discrete nematic phase, whereas TC3 white

displayed a continuous nematic phase with a few isotropic phases. The interactions between organoclays with TLCP molecules at the molecular level enhanced the rigidity of the TLCP molecules, displaying the nematic order structure even at higher temperature. The rheological experiments using CR with a nominal die of $L/D = 30$ and diameter 1.0 mm showed even higher viscosity reduction ability with a wider processing window for TC3 white than for the purified TLCP in the PE matrix. In addition, a much lower yielding stress with a narrower transition window was obtained in the TC3 white/PE blend than in the purified TLCP/PE blend. These findings have promising potential for industrial application to save energy and increase processing efficiency when used in processing such thermoplastics. Mechanism study confirmed that the binary flow model can be applied to describe the rheological behaviours of both blends and shear induced phase transitions and alignment of in-situ formation of fibrils are the primary reasons for viscosity reduction.

Author details

Youhong Tang

Flinders University, Adelaide, South Australia, Australia

Ping Gao

The Hong Kong University of Science and Technology, Kowloon, Hong Kong, China

Acknowledgement

This project was funded by Research Grant Council (RGC) of Hong Kong and Australian Research Council – Discovery Early Career Researcher Award (ARC-DECRA).

6. References

- [1] Romo-Uribe, A.; Lemmon, T. J. & Windle, A. H. (1997). Structure and linear viscoelastic behavior of main-chain thermotropic liquid crystalline polymers. *Journal of Rheology*, Vol. 41, No. 5, pp. 1117-1145, ISSN 0148-6055
- [2] Chan, C. K.; Whitehouse, C. & Gao, P. (1999). The effect of TLCP melt structure on the bulk viscosity of high molecular mass polyethylene. *Polymer Engineering and Science*, Vol. 39, No.8, pp.1353-1364, ISSN 0032-3888
- [3] Whitehouse, C.; Lu, X. H.; Gao, P. & Chai, C. K. (1997). The viscosity reducing effects of very low concentrations of a thermotropic copolyester in a matrix of HDPE. *Polymer Engineering and Science*, Vol 37, No. 12, pp. 1944-1958, ISSN 0032-3888
- [4] Baird, D. G. & Wilkes, G. L. (1983). Sandwich injection-molding of thermotropic copolyesters and filled polyester. *Polymer Engineering and Science*, Vol. 23, No. 11, pp. 632-636, ISSN 0032-3888
- [5] Bafna, S. S.; de Souza, J. P.; Sun, T. & Baird, D. G. (1993). Mechanical-properties of in-situ composites based on partially miscible blend of glass-filled polyetherimide and liquid-crystalline polymers. *Polymer Engineering and Science*, Vol. 33, No. 13, pp. 808-818, ISSN 0032-3888

- [6] Kulichikhin, V. G.; Parsamyan, I. L.; Lipatov, Y. S.; Shumskii, V. F.; Getmanchuk, I. P.; Babich, V. F. & Postema, A. R. (1997). Rheological, mechanical, and adhesive properties of thermoplastic-LCP blends filled by glass fibers. *Polymer Engineering and Science*, Vol. 37, No. 8, pp. 1314-1321, ISSN 0032-3888
- [7] Pisharath, S. & Wong, S. C. (2003). Processability of LCP-nylon-glass hybrid composites. *Polymer Composites*, Vol. 24, No. 1, pp. 109-118, ISSN 0272-8397
- [8] Tchoudakov, R.; Narkis, M. & Siegmann, A. (2004). Electrical conductivity of polymer blends containing liquid crystalline polymer and carbon black. *Polymer Engineering and Science*, Vol. 44, No. 3, pp. 528-540, ISSN 0032-3888
- [9] Tjong, S. C. & Meng, Y. Z. (1999). Microstructural and mechanical characteristics of compatibilized polypropylene hybrid composites containing potassium titanate whisker and liquid crystalline copolyester. *Polymer*, Vol. 40, No. 26, pp. 7275-7283, ISSN 0032-3861
- [10] Lee, M. W.; Hu, X.; Yue, C. Y.; Li, L. & Tam, K. C. (2003). Effect of fillers on the structure and mechanical properties of LCP/PP/SiO₂ in-situ hybrid nanocomposites. *Composites Science and Technology*, Vol. 63, No. 3-4, pp. 339-346, ISSN 0266-3538
- [11] Clarke, S. M.; Rennie, A. R. & Convert, P. (1996). A diffraction technique to investigate the orientational alignment of anisotropic particles: Studies of clay under flow. *Europhysics Letters*, Vol. 35, No. 3, pp. 233-238, ISSN 0295-5075
- [12] Mourchid, A.; Lecolier, E.; van Damme, H. & Levitz, P. (1998). On viscoelastic, birefringent, and swelling properties of laponite clay suspensions: Revisited phase diagram. *Langmuir*, Vol. 14, No. 17, pp. 4718-4723, ISSN 0743-7463
- [13] Schmidt, G.; Nakatani, A. I. & Han, C. C. (2002). Rheology and flow-birefringence from viscoelastic polymer-clay solutions. *Rheologica Acta*, Vol. 41, No. 1-2, pp. 45-54, ISSN 0035-4511
- [14] Pignon, F.; Magnin, A.; Piau, J. M. & Fuller, G. G. (2001). Fibrous clay gels: Extensional flow properties. Dichroism and SALS measurements, *The 2nd International Conference on Self-Assembled Fibrillar Networks*, Autrans, France, Nov 24-28, 2001.
- [15] Zhang, G. L.; Jiang, C. L., Su, C. Y. & Zhang, H. Z. (2003). Liquid-crystalline copolyester/clay nanocomposites. *Journal of Applied Polymer Science*, Vol. 89, No. 12, pp. 3155-3159, ISSN 0021-8995
- [16] Chang, J. H.; Ju, C. H. & Kim, S. H. (2006). Synthesis and characterization of a series of thermotropic liquid crystalline copolyester nanocomposites. *Journal of Polymer Science Part B: Polymer Physics*, Vol. 44, No. 2, pp. 387-397, ISSN 0887-6266
- [17] Vaia, R. A. & Giannelis, E. P. (2001). Liquid crystal nanocomposites: direct intercalation of thermotropic liquid crystalline polymers into layered silicates. *Polymer*, Vol. 42, No. 3, pp. 1281-1285, ISSN 0032-3861
- [18] Huang, W. Y. & Han, C. D. (2006). Dispersion characteristics and rheology of organoclay nanocomposites based on a segmented main-chain liquid-crystalline polymer having pendent pyridyl group. *Macromolecules*, Vol. 39, No. 1, pp. 257-267, ISSN 0024-9297
- [19] Huang, W. Y. & Han, C. D. (2006). Dispersion characteristics and rheology of organoclay nanocomposites based on a segmented main-chain liquid-crystalline

- polymer having side-chain azopyridine with flexible spacer. *Polymer*, Vol. 47, No. 12, pp. 4400-4410, ISSN 0032-3861
- [20] Gao, P., Lu, X. L. & Chai, C. K. (1996). Rheology of low nematic transition temperature thermotropic liquid crystalline copolyester HBA/HQ/SA. *Polymer Engineering and Science*, Vol. 36, No. 22, pp. 2771-2780, ISSN 0032-3888
- [21] Tang, Y. H.; Gao, P.; Ye, L.; Zhao, C. B. & Lin, W. (2010). Organoclay/thermotropic liquid crystalline polymer nanocomposites. Part II: shear-induced phase separation. *Journal of Materials Science*, Vol. 45, No. 16, pp. 4422-4430, ISSN 0022-2461
- [22] Tang, Y. H., Gao, P.; Ye, L. & Zhao, C. B. (2010). Experimental measurement and numerical simulation of viscosity reduction effects in HMMPE containing a small amount of exfoliated organoclay-modified TLCP composite. *Polymer*, Vol. 51, No. 2, pp. 514-521, ISSN 0032-3861
- [23] Chiu, F. C.; Lai, S. M.; Chen, J. W. & Chu P. H. (2004). Combined effects of clay modifications and compatibilizers on the formation and physical properties of melt-mixed polypropylene/clay nanocomposites. *Journal of Polymer Science Part B: Polymer Physics*, Vol. 42, No. 22, pp. 4139-4150, ISSN 87-6266
- [24] Pazzagli, F.; Paci, M.; Magagnini, P.; Pedretti, U.; Corno, C.; Bertolini, G. & Veracini, C. (2000). Effect of polymerization conditions on the microstructure of a liquid crystalline copolyester. *Journal of Applied Polymer Science*, Vol. 77, No. 1, pp. 141-150, ISSN 0021-8995
- [25] Onogi, S. & Asada, T. (1980), *Rheology*, vol. I, Astarita, G., Marrucci, G. & Nicolais, L. (eds.), 127-128, Plenum Press, ISBN 030-640-4656, NY, USA
- [26] Fornes, T. D.; Yoon, P. J.; Keskkula, H. & Paul, D. R. (2001). Nylon 6 nanocomposites: the effect of matrix molecular weight. *Polymer*, Vol. 42, No. 25, pp. 9929-9940, ISSN 0032-3861
- [27] Magda, J. J.; Lee, C. S.; Muller, S. J. & Larson, R. G. (1993). Rheology, Flow instabilities, and shear-induced diffusion in polystyrene solutions. *Macromolecules*, Vol. 26, No. 7, pp. 1696-1706, ISSN 0024-9297
- [28] Macosko, C. W. (1994). *Rheology principles, measurements and applications*, Wiley-VCH, ISBN 1-56081-579-5, NY, USA
- [29] Doi, M. & Edwards, S. F. (1986). *The theory of polymer dynamics*, Oxford Press, ISBN 978-019-8520-33-7, London, UK
- [30] Larson, R. G. (1990). Arrested tumbling in shearing flows of liquid-crystal polymers. *Macromolecules*, Vol. 23, No. 17, PP. 3983-3992, ISSN 0024-9297
- [31] Baek, S. G.; Magda, J. J. & Larson, R. G. (1993). Rheological differences among liquid-crystalline polymers. 1. The 1st and 2nd normal stress differences of PBG solutions. *Journal of Rheology*, Vol. 37, No. 6, pp. 1201-1224, ISSN 0148-6055
- [32] Baek, S. G.; Magda, J. J. & Larson, R. G. (1994). Rheological differences among liquid-crystalline polymers. 2. Disappearance of negative N(1) in densely packed lyotropes and thermotropes. *Journal of Rheology*, Vol. 38, No. 5, pp. 1473-1503, ISSN 0148-6055
- [33] Mather, P. T.; Romo-Uribe, A.; Han, C. D. & Kim, S. S. (1997). Rheo-optical evidence of a flow-induced isotropic-nematic transition in a thermotropic liquid-crystalline polymer. *Macromolecules*, Vol. 30, No. 25, pp. 7977-7989, ISSN 0024-9297

- [34] Han, C. D. & Kim, S. S. (1995). Shear-induced isotropic-to-nematic transition in a thermotropic liquid-crystalline polymer. *Macromolecules*, Vol. 28, No. 6, pp. 2089-2092, ISSN 0024-9297
- [35] de Schrijver, P.; van Dael, W. & Thoen, J. (1996). Surface-induced pretransitional order in the isotropic phase near the isotropic-nematic phase transition. *Liquid Crystals*, Vol. 21, No. 5, pp. 745-749, ISSN 0267-8292
- [36] Chan, C. K.; Whitehouse, C.; Gao, P. & Chai, C. K. (2001). Flow induced chain alignment and disentanglement as the viscosity reduction mechanism within TLCP/HDPE blends. *Polymer*, Vol. 42, No. 18, pp. 7847-7856, ISSN 0032-3861
- [37] Yu, T. H. & Wilkes, G. L. (1996). Influence of molecular weight distribution on the melt extrusion of high density polyethylene (HDPE): Effects of melt relaxation behavior on morphology and orientation in HDPE extruded tubular films. *Journal of Rheology*, Vol. 40, No. 6, pp. 1079-1093, ISSN 0148-6055
- [38] Zhou, H. & Wilkes, G. L. (1998). Orientation-dependent mechanical properties and deformation morphologies for uniaxially melt-extruded high-density polyethylene films having an initial stacked lamellar texture. *Journal of Material Science*, Vol. 33, No. 2, pp. 287-303, ISSN 0022-2461
- [39] Chan, C. K. & Gao, P. (2005) Shear-induced interactions in blends of HMMPE containing a small amount of thermotropic copolyester HBA/HQ/SA. *Polymer*, Vol. 46, No. 24, pp. 10890-10896, ISSN 0032-3861
- [40] Chan, C. K. & Gao, P. (2005). A phenomenological model for the viscosity reductions in blends of HMMPE containing a small quantity of thermotropic liquid crystalline copolyester HBA/HQ/SA. *Polymer*, Vol. 46, No. 19, pp. 8151-8156, ISSN 0032-3861